JOURNAL OF GEOPHYSICAL RESEARCH, VOL. 114, C01S05, doi:10.1029/2008JC004842, 2009

Comparison of model-simulated and observed currents in the central Adriatic during DART

P. J. Martin,[1] J. W. Book,[1] D. M. Burrage,[1] C. D. Rowley,[1] and M. Tudor[2]

Received 31 March 2008; revised 20 October 2008; accepted 18 November 2008; published 10 February 2009.

[1] Numerical simulations of the Adriatic Sea were performed with the Navy Coastal Ocean Model (NCOM) during the Dynamics of the Adriatic in Real Time (DART) Experiments conducted between October 2005 and September 2006. Grid resolution was 1 km. Model forcing included tides, surface fluxes from the Aire Limitée Adaptation Dynamique Développement International (ALADIN) atmospheric model, relaxation to a daily satellite sea surface temperature analysis, extensive river and runoff discharges, and open boundary conditions south of Otranto specified from a global model. Currents predicted by the model were compared with currents from 12 Acoustic Doppler Current Profiler (ADCP) moorings located along a line between the Gargano Peninsula, Italy, and Split, Croatia. The nontidal comparisons were performed with detided currents. Correlations between the model and ADCP currents were highest in the Western Adriatic Current (WAC), which flows southeastward along the Italian coast. Lowest correlations were in the interior of the Adriatic, likely because of instability processes. Correlations between the ALADIN winds and the model and ADCP currents at the mooring locations were also highest in the WAC. For November 2005 through August 2006, the model and ADCP mean WAC transports were 0.321 and 0.304 Sv, respectively, with a temporal correlation of 0.79. Comparison of current variance showed best agreement near the Italian and Croatian coasts. In the interior, the NCOM current variance compared fairly well with that of the ADCPs for November–January but decreased significantly relative to the ADCPs for February–August. Spectral analyses indicate most of the difference in variance to be at periods exceeding 2 days.

Citation: Martin, P. J., J. W. Book, D. M. Burrage, C. D. Rowley, and M. Tudor (2009), Comparison of model-simulated and observed currents in the central Adriatic during DART, *J. Geophys. Res.*, *114*, C01S05, doi:10.1029/2008JC004842.

1. Introduction

[2] There has been a long-standing interest in the physical oceanography of the Adriatic Sea, and reviews are available from *Artegiani et al.* [1997a, 1997b] and *Cushman-Roisin et al.* [2001]. The general circulation of the Adriatic is cyclonic, with a southeastward flow along the western side of the sea, called the Western Adriatic Current (WAC), and a northwestward flow along the eastern side, called the Eastern Adriatic Current (EAC) [*Orlic et al.*, 1992]. Three smaller cyclonic patterns are frequently observed within the overall cyclonic circulation; these are referred to as the North Adriatic Gyre (NAG), the Middle Adriatic Gyre (MAG), and the South Adriatic Gyre (SAG) [*Artegiani et al.*, 1997b; *Poulain*, 2001].

[3] Past theoretical studies have been successful at describing the main features of the oceanography of the Adriatic [e.g., *Hendershott and Rizzoli*, 1976; *Orlic et al.*, 1994]. Recent numerical modeling studies have focused more on the details of the mesoscale variability [*Cushman-Roisin et al.*, 2007; *Korotenko*, 2007].

[4] During the fall and winter of 2002/2003, there was an extensive, international, multidisciplinary study of the northern Adriatic, which included a number of observational and modeling programs [*Lee et al.*, 2005]. These included studies of the response of the Adriatic to strong atmospheric and riverine forcing [*Querin et al.*, 2006; *Peters et al.*, 2007; *Book et al.*, 2007c], sediment transport by the Po and Appennine Rivers, and biological processes, e.g., bottom layer hypoxia. The extensive data that were acquired provide new opportunities for comparison of model results with observations [*Lee et al.*, 2005; *Kuzmic et al.*, 2006; *Martin et al.*, 2006; *Chavanne et al.*, 2007].

[5] More recently, a large, international, collaborative study of the central Adriatic, the Dynamics of the Adriatic in Real Time (DART), was conducted from the fall of 2005 to the fall of 2006. Observational efforts included moored Acoustic Doppler Current Profilers (ADCPs), moored profiling buoys [*Book et al.*, 2007a], Conductivity-Temperature-Depth (CTD) casts, surface drifters [*Haza et al.*, 2007], turbulence profile measurements [*Carniel et al.*, 2008], towed underwater vehicles, remote sensing of temperature and optics, and additional measurements from ships and

[1]Naval Research Laboratory, Stennis Space Center, Mississippi, USA.
[2]Croatian Meteorological and Hydrological Service, Zagreb, Croatia.

0148-0227/09/2008JC004842$09.00

Figure 1. Model domain and bathymetry.

moorings. Numerical modeling efforts included high-resolution meteorological, ocean [*Rixen et al.*, 2007], and wave simulations [e.g., *Dykes et al.*, 2009], with a focus on running multiple models of all three types to provide real-time support and a diversity of predictive methods.

[6] This paper describes a numerical simulation of the Adriatic that was conducted with the Navy Coastal Ocean Model (NCOM) during DART and a comparison of the model-simulated currents with currents measured by ADCPs in the central Adriatic. The simulation of instabilities in the WAC by NCOM during DART and a comparison with observations is discussed by *Burrage et al.* [2009].

[7] The ocean model was run at fairly high (1-km) resolution with atmospheric forcing from Aire Limitée Adaptation Dynamique Développement International (ALADIN) [*Ivatek-Sahdan and Tudor*, 2004], a regional atmospheric model, which also uses fairly high (8-km) resolution. The ocean simulation included tidal forcing and extensive freshwater inflows around the perimeter of the Adriatic.

[8] A main interest was how the currents from the ocean model would compare with the observed currents in the central Adriatic in terms of both predictability and variability. Since much of the mesoscale variability in this region is from current instabilities [*Paschini et al.*, 1993; *Cushman-Roisin et al.*, 2001] that are, to a large degree, nondeterministic (with respect to the model simulations that were conducted), it was expected that the location and timing of particular mesoscale features (e.g., eddies) would not, in general, be accurately predicted. On the other hand, with realistic forcing and bathymetry, the level of variability in a region should be predictable and particular features that are excited by atmospheric forcing and constrained by bathymetry may be predictable to some degree.

[9] The following sections describe (2) the ocean model, (3) the ocean model setup, (4) the ADCP observations, (5) the model results and comparison with observations, and (6) a summary.

2. Ocean Model

[10] The ocean model used here is the Navy Coastal Ocean Model (NCOM) as described by *Martin* [2000], with some improvements as described by *Morey et al.* [2003] and *Barron et al.* [2006]. This model is similar in its physics and numerics to the Princeton Ocean Model (POM) [*Blumberg and Mellor*, 1987], but uses an implicit treatment of the free surface and a hybrid vertical grid with sigma coordinates in the upper layers and (optionally) level coordinates below a user-specified depth.

[11] The model equations include a source term that can be used for river inflows. There are options for higher-order treatment of some terms, e.g., third-order upwind for advection [*Holland et al.*, 1998], which was used for the simulations conducted here. Vertical mixing was computed using the Mellor-Yamada Level 2 scheme [*Mellor and Yamada*, 1974], modified for use over the entire water column. The equation of state used is that of *Mellor* [1991].

3. Ocean Model Setup

3.1. Ocean Model Domain

[12] The ocean model domain consists of the entire Adriatic Sea and includes the Strait of Otranto and a small part of the northern Ionian Sea (Figure 1). A stereographic projection is used, with the long axis of the Adriatic oriented along the y axis of the grid. The horizontal resolution of the grid is 1.02 km.

[13] The vertical grid consists of 32 total layers, with 22 sigma layers used from the surface down to a depth of 291 m and level coordinates used below 291 m. Hence, the grid is like a regular sigma coordinate grid in water shallower than 291 m and is similar to a level grid in deeper water. The vertical grid is uniformly stretched from the

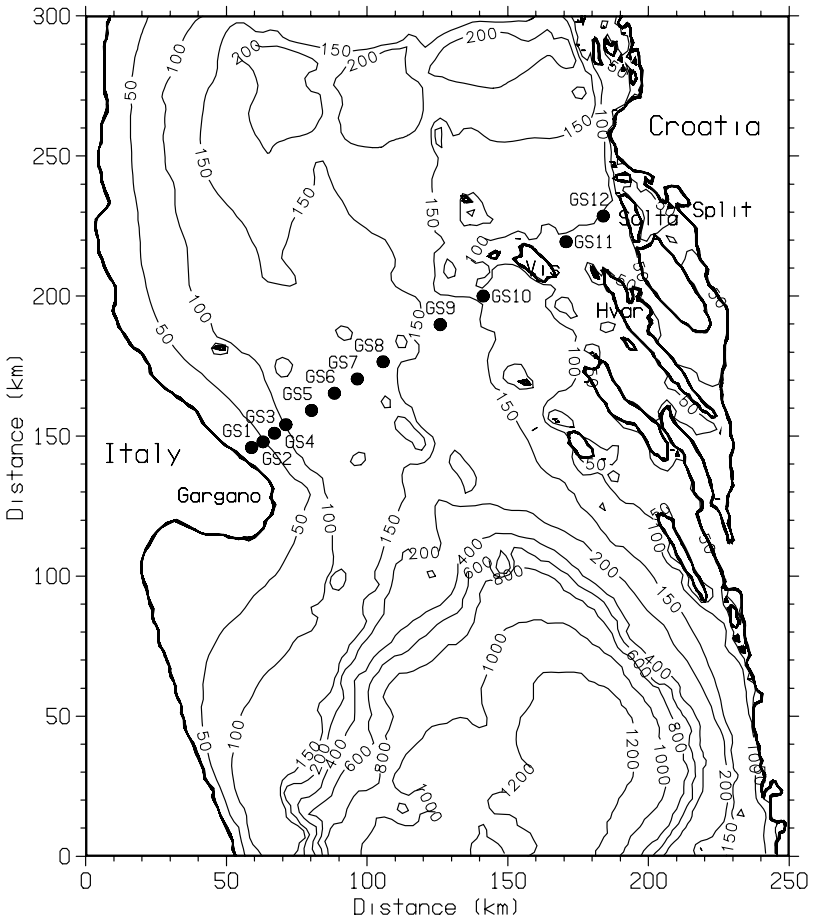

Figure 2. Model bathymetry in central Adriatic and GS mooring locations (black dots).

surface downward with a maximum thickness of the upper layer of 2 m and a maximum depth of 1262 m. The minimum water depth was set to 2 m.

[14] Figure 1 shows the bathymetry for the entire domain and Figure 2 shows the bathymetry in the central Adriatic in more detail. The bathymetry was derived from a database developed by the U.S. Naval Oceanographic Office and nautical chart soundings. The land-sea boundary was derived from the Generic Mapping Tools (GMT) vector shoreline.

3.2. Initial and Boundary Conditions

[15] Initial conditions (ICs) for sea surface height (SSH), current velocity (u, v), temperature (T), and salinity (S) for 1 January 2005 were interpolated from a hindcast of a global version of NCOM that was developed at the U.S. Naval Research Laboratory (NRL) [*Barron et al.*, 2004] and is currently being run at the U.S. Naval Oceanographic Office. Boundary conditions (BCs) at the open boundary in the northern Ionian Sea were provided by daily values of SSH, u, v, T, and S from the global model. The numerical treatment of the BCs includes the *Flather and Proctor* [1983] radiative BC for the SSH and depth-averaged normal velocity, *Orlanski* [1976] radiation conditions for the tangential velocity and T and S, and a relaxation to the T and S fields of the global model near the open boundary. The normal baroclinic velocity at the open boundary is computed using the model's full velocity equation, except that advection is only computed normal to the boundary (with a first-order-upwind scheme).

3.3. Tidal Forcing

[16] Tidal forcing was imposed by computing the tidal SSH and depth-averaged normal and tangential transport (velocity times depth) at the open boundaries from tidal harmonic data obtained from the Oregon State University (OSU) tidal databases, which are derived from satellite altimetry data [*Egbert and Erofeeva*, 2003]. The tidal BCs are linearly combined with the BCs from global NCOM (which does not include tides). Data from the OSU Mediterranean tidal database were used for the K_1, O_1, M_2, and S_2 constituents (the only constituents this database contains) and data from the OSU global database were used for P_1, Q_1, K_2, and N_2. Tidal potential forcing for these eight constituents was used in the interior of the model domain. It is noted by *Cushman-Roisin et al.* [2001] that all these constituents (except for Q_1) are needed to adequately represent the tides in the Adriatic.

3.4. Atmospheric Forcing

[17] Atmospheric forcing was obtained from the ALADIN model, which is run on a domain covering the Adriatic Sea and adjoining countries by the Croatian Meteorological and Hydrological Service [*Ivatek-Sahdan and Tudor*, 2004]. This model uses a Lambert conformal grid with a horizontal

Table 1. Depth Range and Depth Cell Size of Currents Measured by ADCPs[a]

Mooring	Upper	Lower	Cell Size
GS1	2	16	0.5
GS2	3	31	0.5
GS3	10	78	2
GS4	10	94	3
GS5	12	111	3
GS6	14	124	3
GS7	14	122	3
GS8	14	124	5/3
GS9	20[b]	165	5
GS10	15	140	5
GS11	9	88	2
GS12	9	95	2

[a]Unit is in meters.
[b]Only 15% of this ADCP's data are good at this depth level.

resolution of about 8 km and is nested within the ARPEGE global atmospheric model [*Courtier and Geleyn*, 1988].

[18] The atmospheric forcing consisted of hourly fields of surface air pressure, wind stress, solar radiation, net longwave radiation, and precipitation from ALADIN. Latent and sensible heat fluxes were computed with standard bulk formulas using the ALADIN 10-m wind speed and 2-m air temperature and humidity and the ocean model sea surface temperature (SST). The stability-dependent *Kondo* [1975] drag coefficient was used for the bulk flux calculations with neutral values of 0.0014 and 0.0011 for the latent and sensible heat fluxes, respectively. The evaporative moisture flux was derived from the bulk-calculated latent heat flux. Note that the use of bulk formulas, the ocean model SST, and the ALADIN air temperature to compute the latent and sensible heat fluxes provides an indirect relaxation of the ocean model SST to the SST analysis used by ALADIN.

[19] The ocean model SST was also relaxed to a daily MCSST analysis for the Adriatic Sea (conducted at NRL) to improve the accuracy of the predicted SST. This SST relaxation was implemented using an additional surface heat flux computed as the difference between the SST from the analysis and the ocean model SST, multiplied by a rate of 0.5 m/d.

3.5. River and Runoff Inflows

[20] Rivers are input into the ocean model as a volume source with zero salinity and a specified vertical distribution and temperature. Since real-time river temperatures were not available, they were specified from a monthly climatology for the Adriatic at the location of the river mouth. River and runoff inflows for the Adriatic were taken from the monthly climatological database of *Raicich* [1994]. This database includes discharges for 39 specific rivers and general runoff inflows along several sections of the Adriatic coastline. For input to the model, the runoff inflows were distributed along the appropriate part of the coast. The total

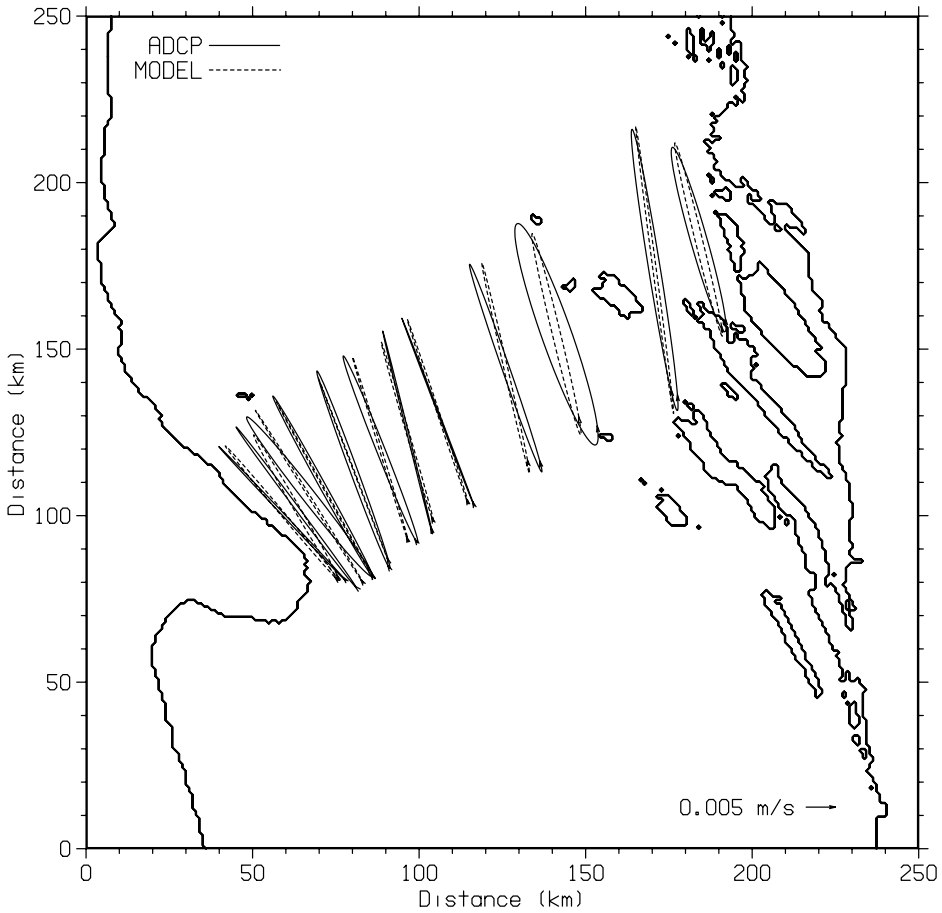

Figure 3. Model and ADCP M_2 tidal ellipses for depth-averaged current.

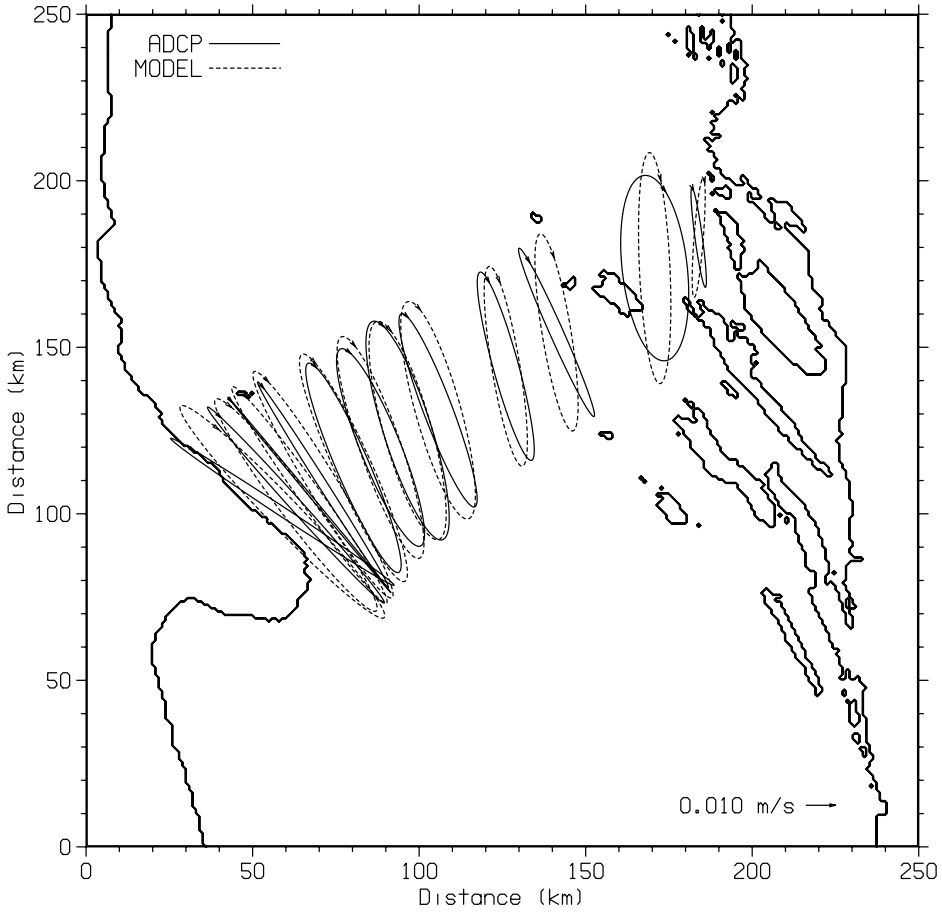

Figure 4. Model and ADCP K_1 tidal ellipses for depth-averaged current.

annual mean discharge for the Adriatic from Raicich's database is 5700 m^3/s.

[21] Daily observed discharge values for the Po River (provided courtesy of ARPA-SIM, Emilia Romagna) were used starting 1 December 2005. The Po is the largest of the Adriatic rivers, with a mean discharge of about 1575 m^3/s [*Raicich*, 1994]. The mean observed discharge of the Po from December 2005 through August 2006 was 687 m^3/s versus 1527 m^3/s for climatology [*Raicich*, 1994]; hence, the Po discharge was significantly lower than its mean value. The discharge from the Po was spread over 5 different locations around the Po Delta, with each location getting a fixed fraction of the Po's total discharge.

3.6. Model Simulation

[22] The ocean model was run from 1 January 2005 to the end of September 2006, with a time step of 150 s. During the two main field experiments (2–25 March and 16 August to 23 September 2006), the model was run daily in a hindcast/forecast mode with a 48-h hindcast followed by a 48-h forecast and the output was posted to the DART project web site maintained at the NATO Undersea Research Center (NURC) for access by other researchers, including those aboard ship taking part in the field experiments.

[23] The full, three-dimensional model fields (u, v, T, and S) were saved every 3 h and hourly values of the model fields were saved at the surface and at the mooring locations (Figure 2). The results reported here use only the model hindcast fields.

4. Current Observations

[24] To realize the research goal of better understanding the accuracy of NCOM and other high-resolution coastal ocean models over various space and time scales in regions of complex topography and dynamics, the DART project produced and utilized a comprehensive observational data set for studying coastal ocean processes. A major focus was

Table 2. Percent of Total ADCP Current Variance due to Eight Main Tidal Constituents at Mooring Locations

Mooring	10-m Depth	Bottom
GS1	10.2	9.9
GS2	7.0	11.9
GS3	6.8	12.5
GS4	7.5	16.1
GS5	5.6	18.2
GS6	4.9	12.9
GS7	4.7	11.8
GS8	4.4	8.6
GS9	7.2	7.3
GS10	4.9	8.7
GS11	5.5	10.2
GS12	2.6	5.1

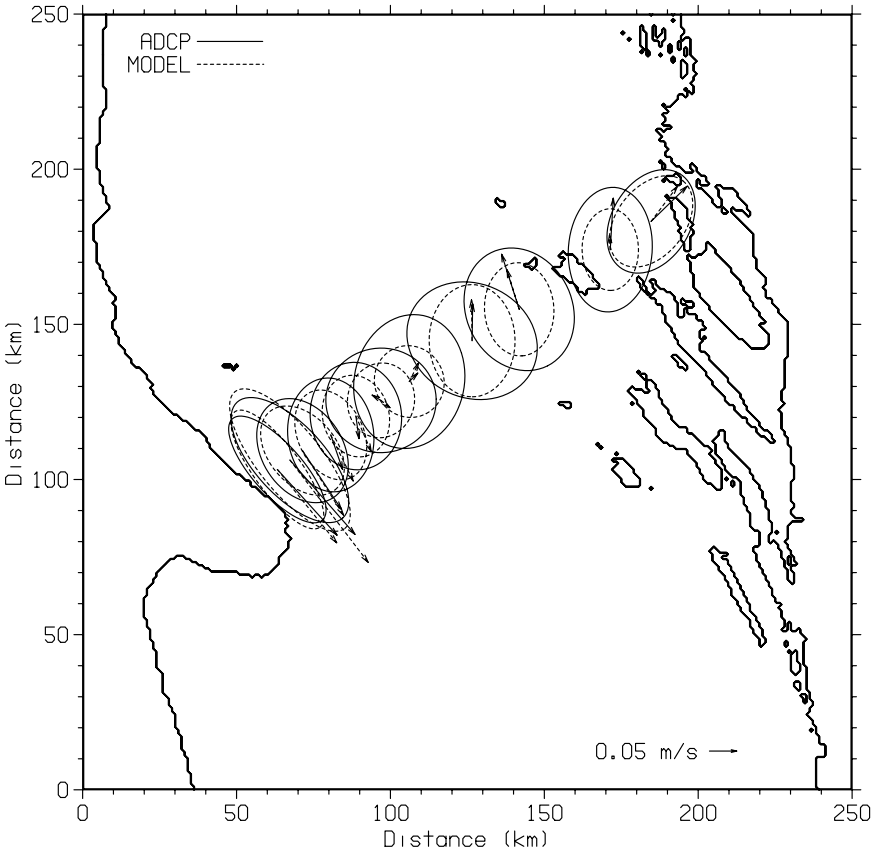

Figure 5. Detided model and ADCP mean current vectors and STD current ellipses at 20 m for period November 2005 through August 2006.

on an array of long-term ADCP moorings augmented by additional moorings during two, month-long experiments in winter and summer. This paper compares the long-term ADCP observations with the NCOM-predicted currents.

[25] A string of bottom-mounted, upward looking ADCP moorings (GS1–GS12) were deployed by NRL along a line spanning the Palagruža Sill between the Gargano Peninsula, Italy and Split, Croatia (Figure 2). Measurements were made from October 2005 to September 2006 (11 months) utilizing the trawl-resistant Barny Sentinel design [*Perkins et al.*, 2000] to provide protection from the heavy fishing activity of this region. To counter corrosion development, the moorings were recovered, refurbished, and redeployed midway through the experiment, creating a 0–21 day time gap in the records (a typical gap was 6 days). Despite this, GS11 failed on 22 June because of corrosion and GS9 failed on 30 July because of a faulty mechanical part. All the other mooring durations spanned a 10–11 month time period. In addition to current measurements throughout the water column, the moorings also recorded the pressure, temperature, and salinity at the bottom.

[26] Because of standard ADCP ringing and surface sidelobe contamination, measurements were not taken or were inaccurate in zones near the bottom and near the sea surface, respectively. The width of these zones varies according to the ADCP frequency (for this study ranging from 1200 kHz to 300 kHz), deployment depth (from 17 m to 173 m), and depth cell resolution (from 0.5 to 5 m). Therefore, the distance of the uppermost depth cell from the sea surface ranged from 1.5 to 15 m and the distance from the lowest depth cell to the sea bottom ranged from 1.5 to 8 m. Because of its greater deployment depth, GS9 was an exception to this, and few accurate current measurements were made by GS9 closer than 45 m from the sea surface. Table 1 lists further details.

[27] The accuracy of the current measurements also varies according to sampling strategy, location, and depth cell size. Teldyne/RD Instruments ADCPs have four acoustic beams and random horizontal velocity error can be estimated from the standard deviation of the weighted difference time series between two independent measurements of vertical velocity. This estimate varied through the DART array from a low of ±0.9 cm/s to a high of ±5.0 cm/s for individual depth cells. In addition to these random errors (which can be sharply reduced by averaging or filtering), there is likely an ADCP bias, estimated by Teldyne/RD Instruments to be ±0.5% of the current magnitude plus ±0.5 cm/s for 300 kHz ADCPs and ±0.3% of the current magnitude plus ±0.3 cm/s for 600 kHz and 1200 kHz ADCPs.

[28] Finally, an additional error (estimated to be ±0.8 cm/s using the sampling error estimate procedure detailed by *Book et al.* [2007b] but adjusted for the DART ADCP parameters) could be present in the data because of the fact that the measurements were made using 44–114 s bursts at 1 Hz every 15 min instead of being evenly sampled over the interval. However, even greater errors can be induced by aliased surface wave orbital velocities in spread sampling strategies and, in fact, these could be present during the first

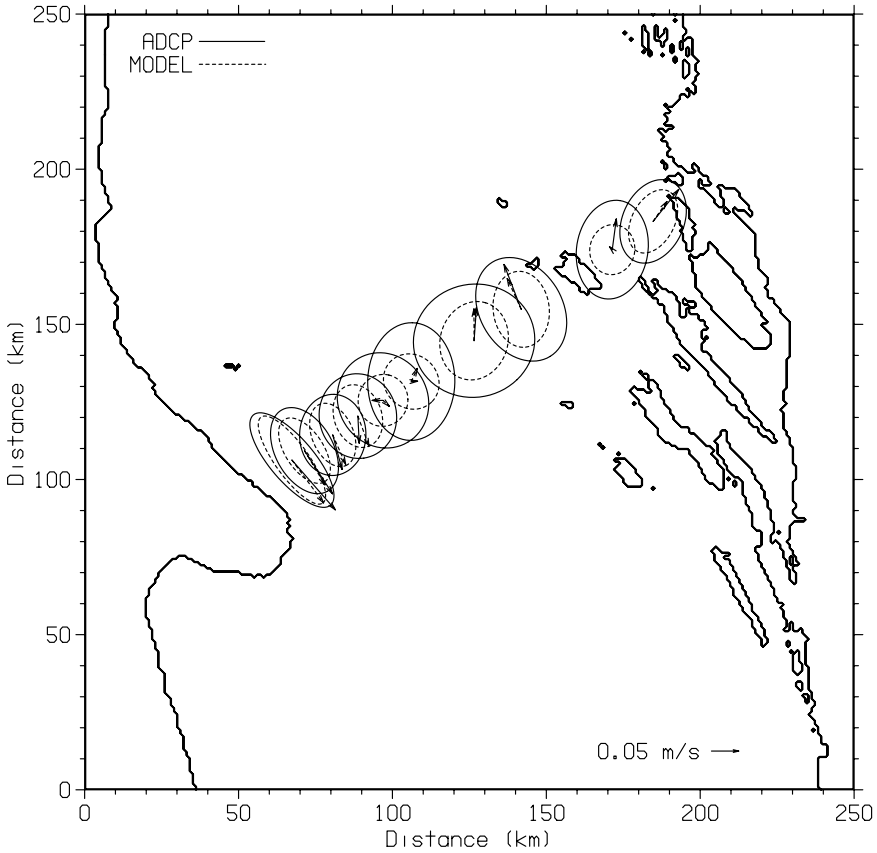

Figure 6. Detided model and ADCP mean current vectors and STD current ellipses at 50 m for period November 2005 through August 2006.

half of the GS1 record, since it alone used such a strategy, sampling at 0.1 Hz over 15 min.

5. Results

5.1. Tidal Currents

[29] Tidal analysis of the model and observed time series data was performed using a least-squares fit to the eight tidal constituents used for the model simulation (see section 3.3). Comparison of the model tidal SSH with data from International Hydrographic Organization (IHO) stations and comparison of tidal currents with ADCP measurements taken in the northern Adriatic during ACE in 2002/2003 were presented by *Martin et al.* [2006] and *Book et al.* [2009] and showed good agreement.

[30] During DART, tidal currents for the eight tidal constituents were computed from the ADCP data and from the hourly model output at the GS mooring locations (Figure 2). Figures 3 and 4 show plots of the model and ADCP M_2 and K_1 tidal ellipses computed from the depth-

Table 3. Model Mean, RMS, and Correlation Errors With Respect to ADCP Measured Velocities at 20 m[a]

	Principal Axis			Minor Axis		
Mooring	Mean	RMS	Correlation Error	Mean	RMS	Correlation Error
GS1	−2.5	9.0	0.568	−1.8	6.4	0.082
GS2	−0.7	12.2	0.544	−0.9	6.1	0.109
GS3	−5.2	14.3	0.626	−1.5	8.8	0.025
GS4	−1.1	10.1	0.490	−0.3	9.2	0.115
GS5	−2.5	11.5	0.325	1.3	9.8	0.060
GS6	−2.6	11.7	0.167	1.8	9.7	0.153
GS7	0.9	11.7	0.052	−4.1	11.6	0.163
GS8	−1.9	13.1	0.154	−0.4	12.0	0.038
GS9	0.8	13.1	0.003	0.3	11.3	0.207
GS10	−3.0	12.0	0.352	0.1	11.3	0.057
GS11	−6.9	13.9	0.223	−0.1	9.1	0.041
GS12	−1.0	12.6	0.188	−1.5	8.9	0.160

[a]Velocities are detided. Errors are computed along the local principal and minor variance axes. Mean and RMS errors are in cm/s.

Table 4. Monthly Variance of Model and ADCP Currents Averaged Over Moorings GS5–10 at 20-m Depth for November 2005 to August 2006[a]

Month	Model	ADCP
Nov	70	130
Dec	226	215
Jan	189	264
Feb	68	253
Mar	60	308
Apr	67	217
May	30	193
Jun	42	182
Jul	36	56
Aug	40	84

[a]Unit is in cm^2/s^2.

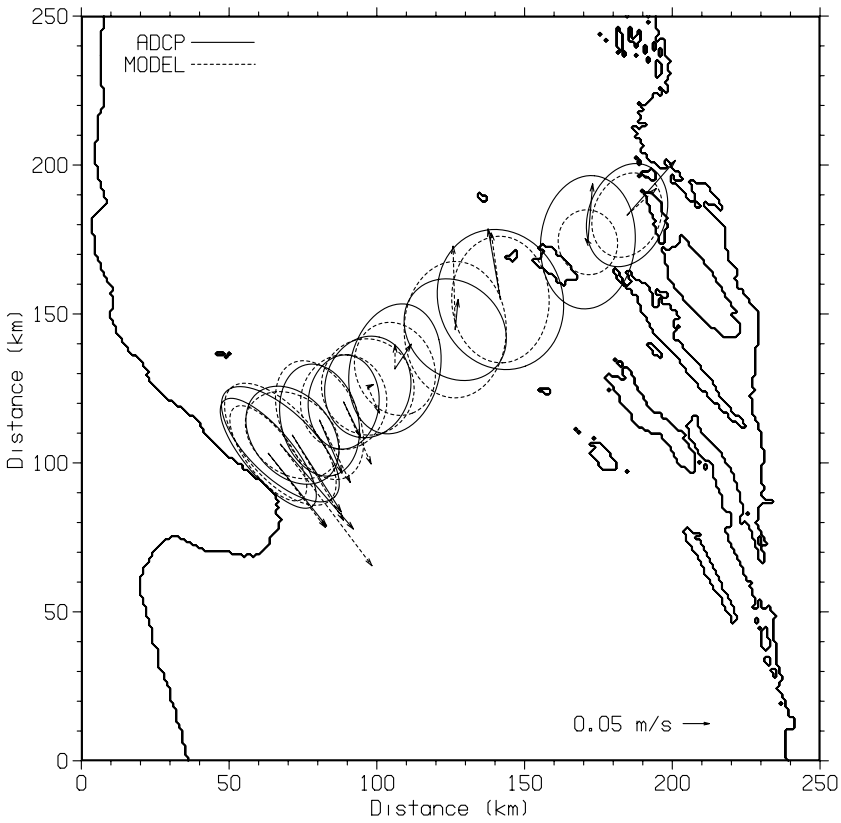

Figure 7. Detided model and ADCP mean current vectors and STD current ellipses at 20 m for period November 2005 through January 2006.

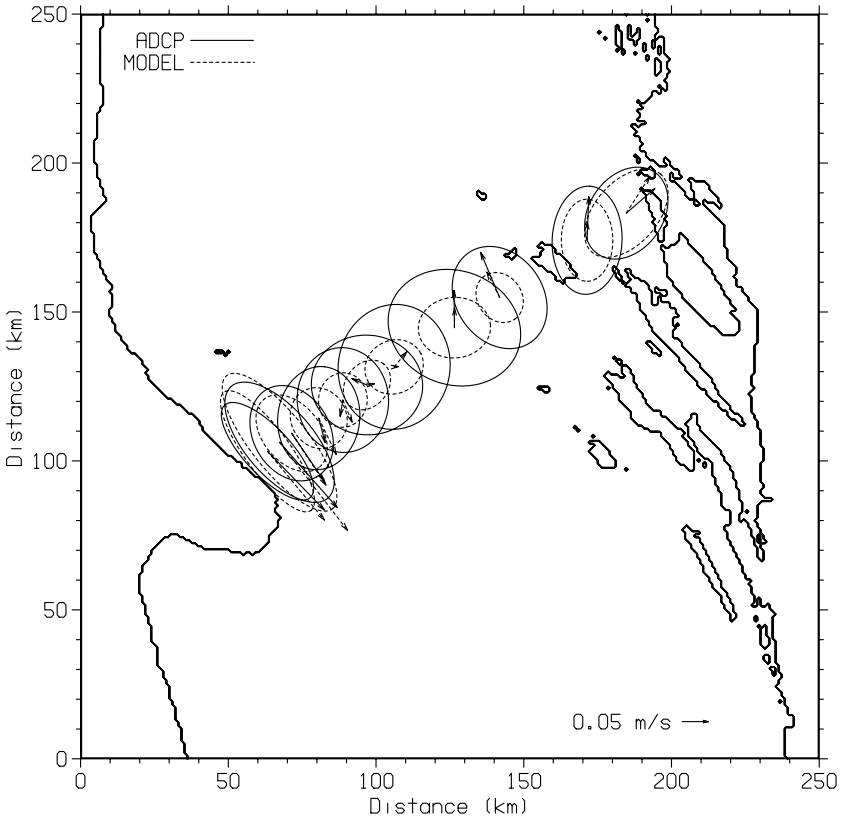

Figure 8. Detided model and ADCP mean current vectors and STD current ellipses at 20 m for period February through August 2006.

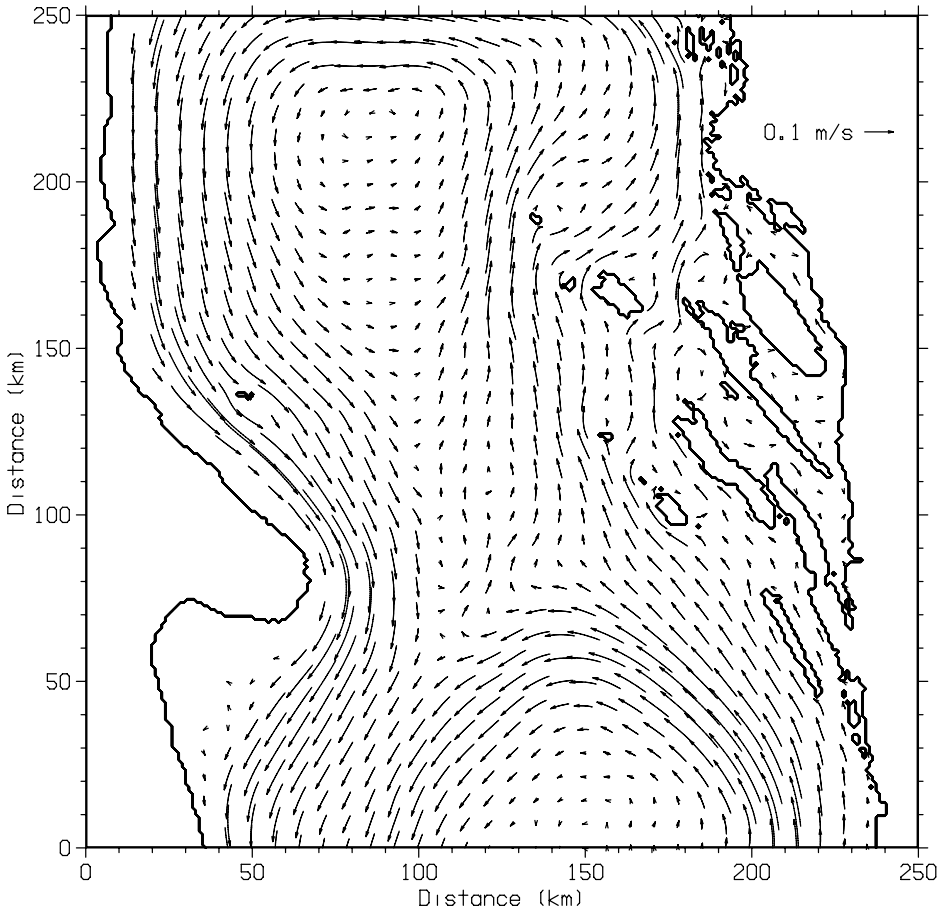

Figure 9. Time-averaged model current at 20-m depth for period November 2005 through August 2006.

averaged currents (note that the velocity scaling in these two plots is different). There is fairly good agreement in the amplitude and orientation of the tidal ellipses at all the GS moorings. The tidal currents for the S_2 and O_1 constituents (not shown) also agree well with the mooring currents. The percentage of the total variance of the ADCP currents due to the eight tidal constituents (Table 2) ranges from a low of 2.6% near the surface at GS12 to a high of 18.2% near the bottom at GS5. These percentages tend to be higher near the bottom where the total currents are weaker.

5.2. Mean Currents and STD Ellipses

[31] The remainder of the model and ADCP comparisons in this paper are made with detided currents. Figures 5 and 6 show plots of the 20- and 50-m mean current vectors and standard deviation (STD) ellipses for the model and ADCP detided currents at the mooring locations computed for the period November 2005 through August 2006 (except that the observations at GS9 and GS11 end on 30 July and 22 June, respectively, and the calculation of statistics at these moorings ends on these dates). Note that the scaling of the STD ellipses in Figures 5 and 6 is different from the scaling of the tidal ellipses in Figures 3 and 4.

[32] The model mean currents are generally in fairly good agreement with the observed mean currents (Table 3). However, the model mean current in the WAC near the Italian coast at GS3 at 20-m depth is noticeably larger than observed and the model mean current at GS11 at both 20 and 50 m is significantly smaller than observed.

[33] At 20-m depth, the magnitude and orientation of the STD ellipses of the detided model currents agree quite well with those of the observed currents in the WAC and near the Croatian coast (Figure 5). However, in the interior of the Adriatic and at deeper depths (Figure 6), the model STD ellipses tend to be noticeably smaller than observed.

[34] Calculation of the model and observed current variance by month for moorings GS5–10 at 20-m depth shows a significant drop in the model current variance between January and February 2006 (Table 4), whereas the observed variance at these moorings remains relatively high until July. Figures 7 and 8 show plots of the 20-m mean current vectors and STD ellipses for November 2005 through January 2006 and for February through August 2006, respectively. These two plots show the large decrease in the size of the model STD ellipses in the interior of the Adriatic for the later (February–August) time period; the observed STD ellipses show much less of a difference. The agreement of the model and observed STD ellipses at moorings GS5–10 is significantly better for the earlier (November–January) period.

[35] Some model experiments were conducted to investigate whether some aspects of the model simulation (the type of vertical coordinate, the number of vertical layers, the strength of the SST relaxation, the particular bathymetry)

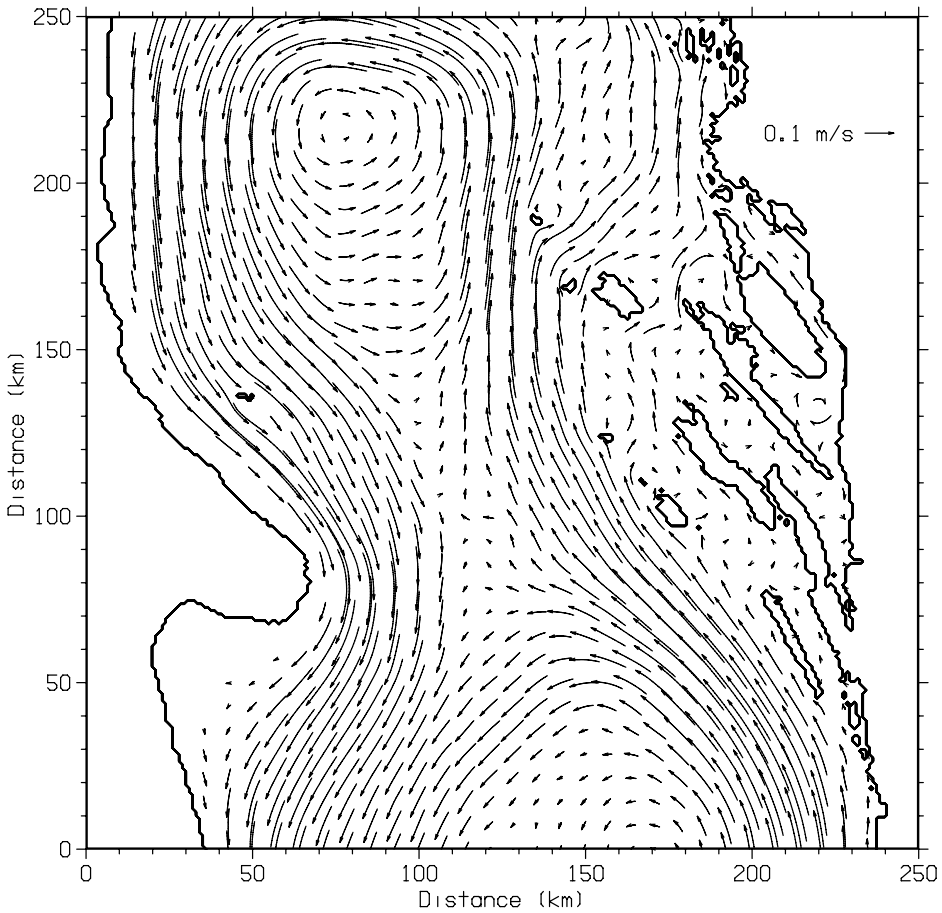

Figure 10. Time-averaged model current at 20-m depth for period November 2005 through January 2006.

might be the cause of the low model variance. Additional hindcasts were run with different types of vertical coordinates (including generalized sigma coordinates and primarily level coordinates), an increased number of vertical layers, SST relaxation turned off, and a different bathymetry database. However, these alternative model simulations gave current variances similar to the original run; hence, the cause of the low model variance in the interior for February–August was not determined.

[36] Figure 9 shows a plot of the time-averaged model current at 20-m depth for November 2005 through August 2006. The main features of this time-averaged circulation are generally consistent with the 9-year mean (August 1990 to July 1999) computed from drifter observations by *Poulain* [2001], i.e., a relatively strong EAC and WAC, with the EAC being noticeably broader than the WAC in the central Adriatic, and a relatively strong MAG and SAG, with the main flow on the northwest side of these gyres being primarily from the east side of the Adriatic to the west side and following a fairly straight path across the Adriatic on the northwest side of the MAG and a more curved path on the northwest side of the SAG. *Poulain* [2001] shows current magnitudes in the EAC and WAC of 10–20 cm/s; Figure 9 shows slightly lower values, though these are at 20-m depth rather than near the surface. Both *Poulain* [2001] and Figure 9 show acceleration of the WAC as it rounds Gargano Peninsula, with maximum mean current speeds of about 25 cm/s.

[37] Figures 5–8 show that the model mean current at GS12 is directed toward the Croatian coast in agreement with the observed mean current, rather than parallel to the coast as might be expected. The behavior of the model mean current near GS12 can be seen in Figure 9, which shows that the model mean current flows around the western end of Hvar Island (just southeast of GS12) toward Solta Island and does not turn off this path to a direction more parallel to the coast until fairly close to Solta. Animations of the model current show a small, anticyclonic eddy frequently being formed between Hvar and Solta as the EAC rounds Solta and a suggestion of this eddy can be seen in Figure 9.

[38] Figures 10 and 11 show plots of the time-averaged model current at 20 m for November 2005 through January 2006 and for February through August 2006, respectively. All the main circulation features are noticeably stronger for November–January. For February–August, there is a return flow from the northwest side of the SAG northward toward the Croatian Islands on the eastern side of the central Adriatic, which rejoins the branch of the EAC that follows the eastern coast. In summer, the time-averaged flow shows a southward flow along the eastern coast in the southern part of the Adriatic due to an elongated recirculation gyre between the SAG and the eastern coast (not shown).

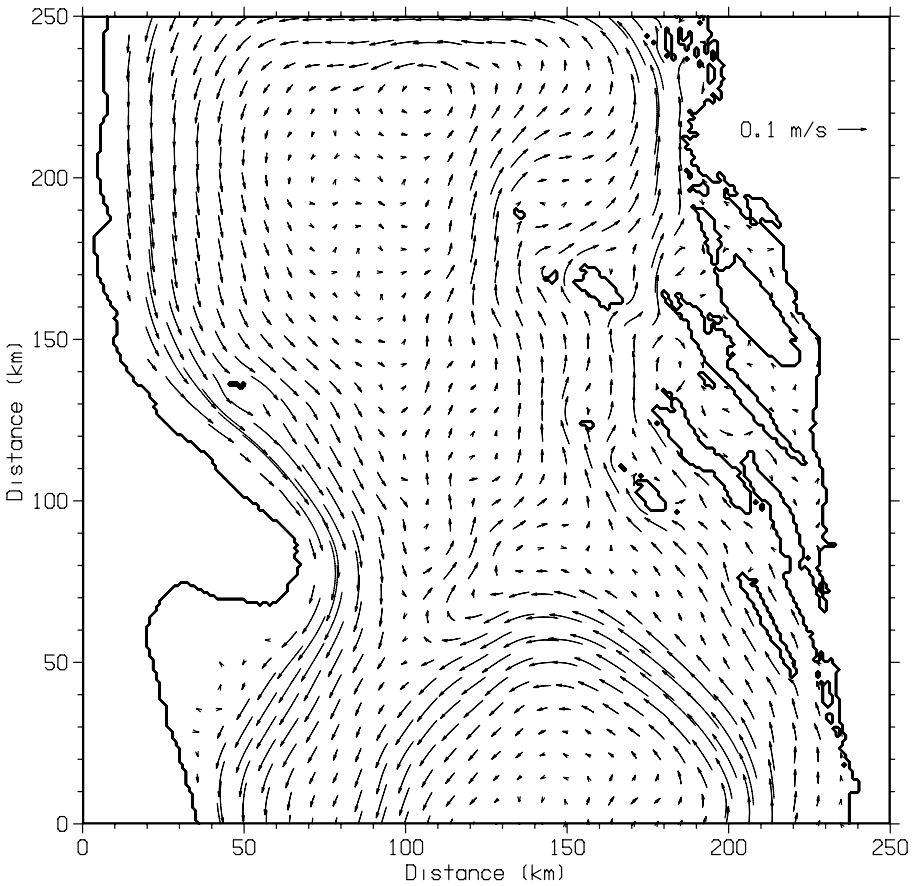

Figure 11. Time-averaged model current at 20-m depth for period February through August 2006.

5.3. Current Spectra and Variance

[39] Figures 12 and 13 show spectra for the model and observed detided currents for the period November 2005 through August 2006 at GS2 and GS10 at 20 m. These two moorings were selected as representative of locations in the WAC and in the interior of the central Adriatic, respectively.

[40] Both moorings show less variance in the model currents than was observed at frequencies above 2 cycles/d, and this was the case at all the moorings. However, the fraction of the total current variance at these high frequencies is small.

[41] At lower frequencies, the model and observed current variance agree fairly well at GS2 and the other moorings (GS1–4) in the WAC, but the model current variance is significantly lower than observed at GS10 and the other moorings (GS5–11) in the interior.

[42] Figures 14 and 15 show cumulative current variance versus frequency at GS2 and GS10 corresponding to the spectra plotted in Figures 12 and 13. Also plotted is the difference between the observed and model-simulated cumulative variance. These plots show that most of the variance and most of the difference in variance between the observed and model currents occurs at low frequencies below about 0.5 cycles/d (i.e., for periods longer than 2 days).

5.4. Current Time Series

[43] Figures 16 and 17 show a comparison of the model and ADCP current time series at GS2 and GS10 at 20-m depth for April–May 2006. The currents are plotted along the axes of maximum and minimum variance, which approximately correspond to the alongshore and cross-shore directions, respectively. The model captures much of the alongshore variability observed at GS2.

[44] Both the model and observed current at GS10 show a significant amount of variability due to inertial waves. Figure 13 shows a noticeable peak near the inertial frequency in the power spectra at GS10 and the energy at the inertial frequency for the observed and simulated currents is similar. The other interior moorings, GS4 to GS9, all show noticeable peaks in their power spectra at the inertial frequency (not shown). The inertial energy is weaker at the moorings near the coast.

[45] The large current variability observed at GS10 at the beginning of April in Figure 17 does not occur in the model simulation. For the period February–August, many other stronger events can be seen in the observed currents than in the model-simulated currents, which is consistent with the low-frequency variability of the observed currents being higher than for the model currents at GS10.

5.5. WAC Transport

[46] Figure 18 shows a time series of the net transport within the WAC computed from the model and ADCP currents using data from moorings GS1–7. For consistency, both transports were computed in the same way using currents just at the mooring locations. The transports in

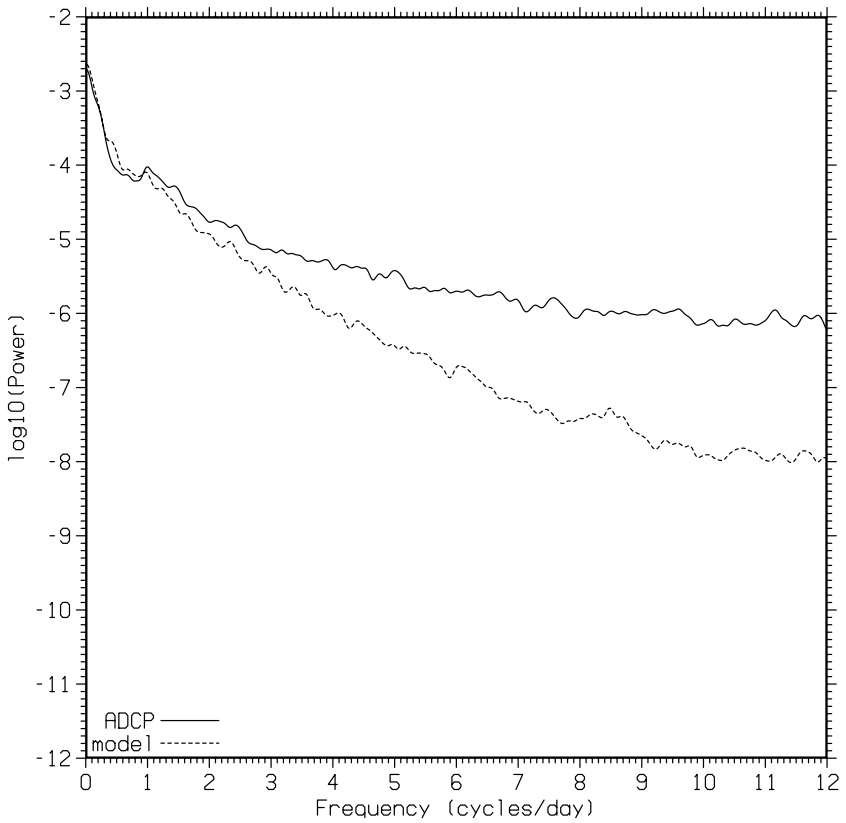

Figure 12. Power spectrum of detided model and ADCP current at GS2 at 20 m for period November 2005 through August 2006.

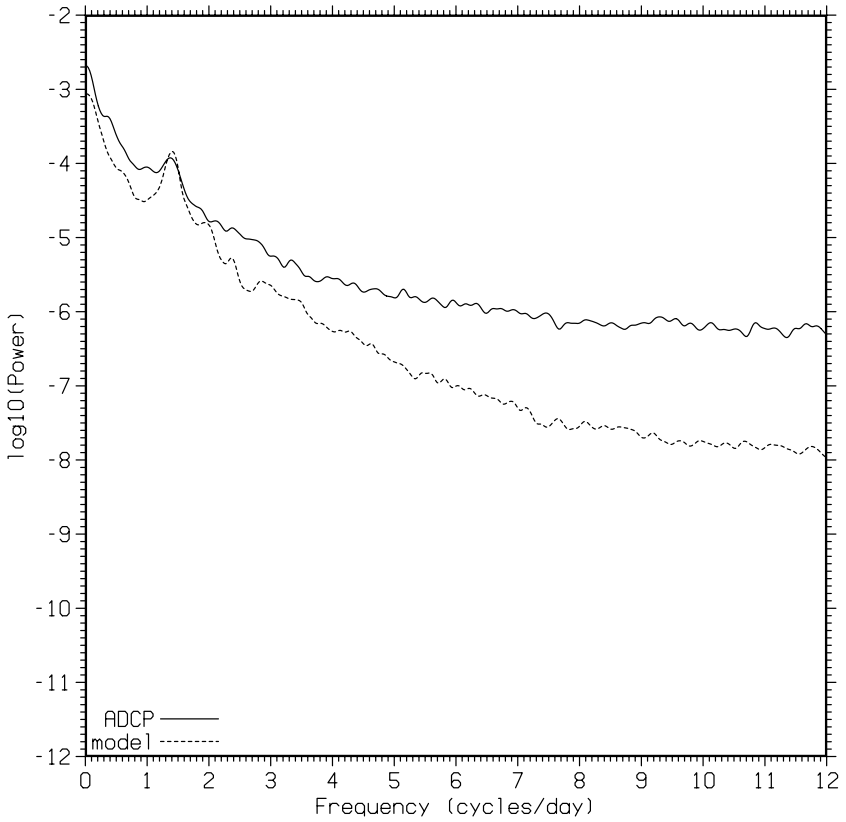

Figure 13. Power spectrum of detided model and ADCP current at GS10 at 20 m for period November 2005 through August 2006.

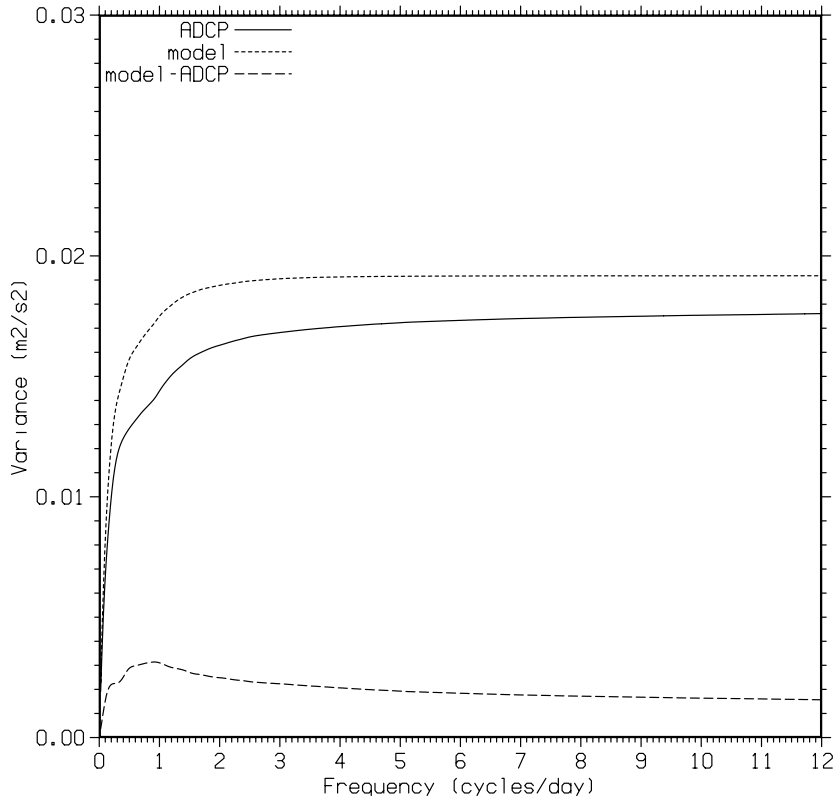

Figure 14. Cumulative variance versus frequency for detided model and ADCP current at GS2 at 20 m for period November 2005 through August 2006.

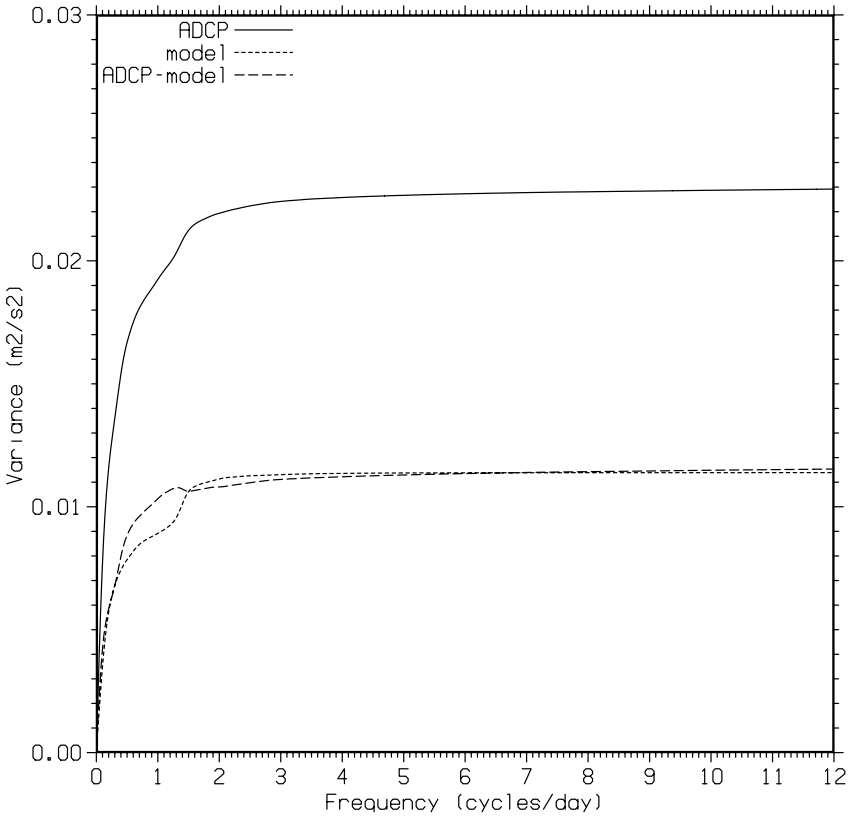

Figure 15. Cumulative variance versus frequency for detided model and ADCP current at GS10 at 20 m for period November 2005 through August 2006.

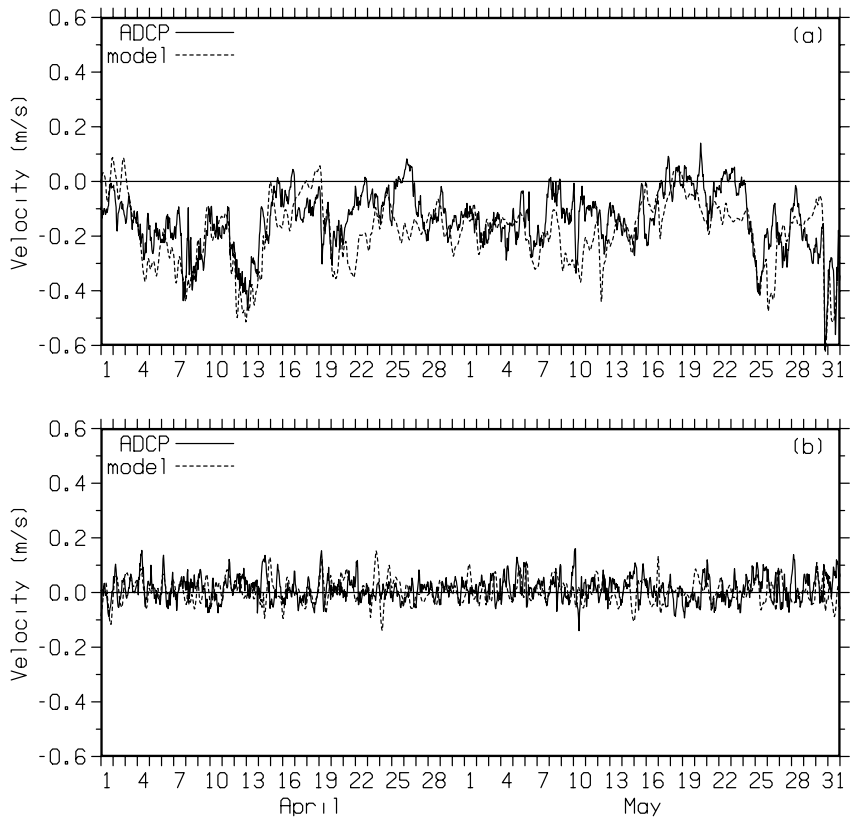

Figure 16. Detided model and ADCP 20-m currents at GS2 for April–May 2006 along axes of (a) maximum and (b) minimum variance.

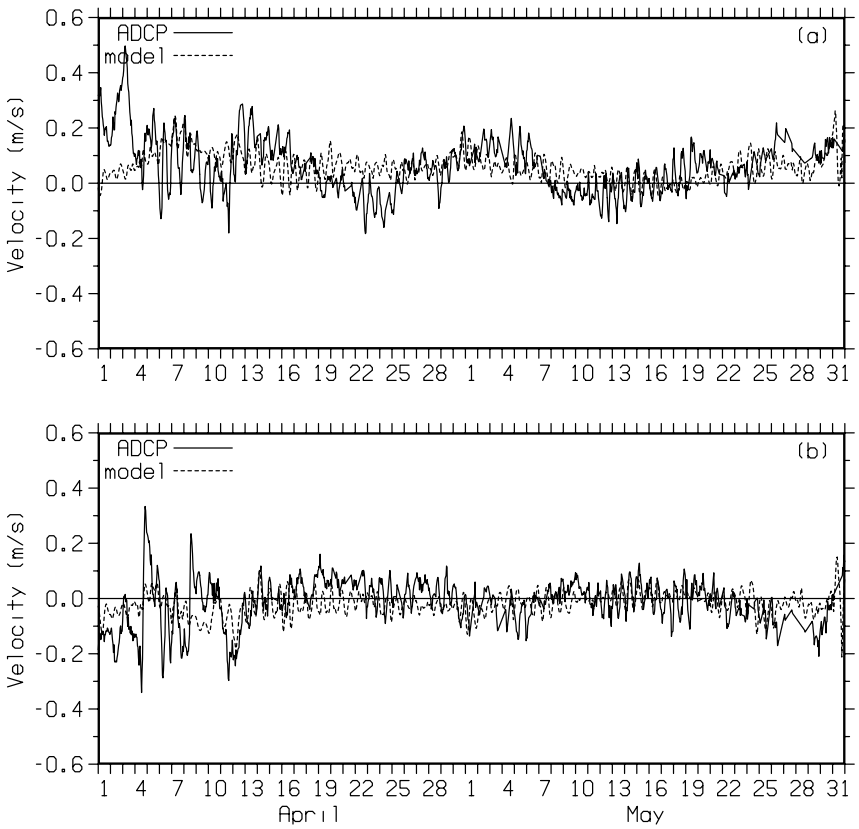

Figure 17. Detided model and ADCP 20-m currents at GS10 for April–May 2006 along axes of (a) maximum and (b) minimum variance.

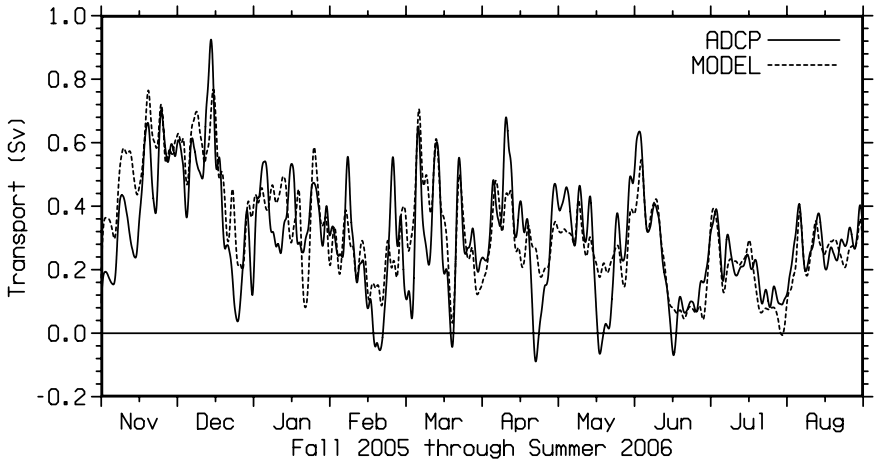

Figure 18. Transport in WAC computed from model and ADCP currents at the mooring locations.

Figure 18 were low-pass filtered with a 72-h Butterworth filter. The correlation between the filtered transport time series is 0.79 (the correlation for the unfiltered time series is 0.73). The mean transports for November 2005 through August 2006 are 0.321 and 0.304 Sv for the model and ADCP currents, respectively.

[47] The time mean WAC transport near the GS mooring line for this 10-month period was also computed using the full model velocity fields. This transport was computed between the coast and a fixed location about 52-km offshore, the distance offshore being chosen to yield the maximum mean transport for the 10-month period. This offshore location used to terminate the transport calculation is close to GS7, and the computed maximum mean transport is 0.330 Sv, i.e., only slightly larger than the transport estimated using the model currents at just the mooring locations.

[48] The WAC transport computed from the full model velocity fields near the GS mooring line was cross correlated with the ALADIN wind stress fields to provide an indication of which wind stress forcing most affected the WAC transport [*Pullen et al.*, 2003; *Book et al.*, 2005]. The ALADIN wind stress fields were spatially averaged within 0.5° longitude-latitude bins. Both the wind stress and WAC transport time series were low-pass filtered with a 24-h Butterworth filter. The cross correlation (CC) was computed between the WAC transport and the wind stress projected at all possible angles (in 1° increments).

[49] Figure 19 shows a contour plot of the maximum CC within each longitude-latitude box taken over all the wind stress directions and time lags from 0 to 48 h. The highest CC of 0.51 occurs near the central Croatian coast and the lag of the wind stress associated with this maximum is about 30 h. Regions where the CC exceeds 0.4 occur along the Croatian coast, along the Italian coast north of Gargano Peninsula, and in the northern Adriatic. The time lags associated with the maximum CC in these areas tends to increase with distance from where the transport was computed near Gargano Peninsula, varying from 10 h along the Italian coast north of Gargano to 34 h in the northern Adriatic. Use of longer temporal filters for the WAC transport yields higher CC values, e.g., 0-, 24-, 48-, and 72-h filters give maximum CCs of 0.47, 0.51, 0.56, and 0.60, respectively.

[50] The wind directions that give the highest CC are indicated by the arrows in Figure 19 (the arrows are only plotted where the maximum CC exceeds 0.3). The wind directions that give the maximum CC in the northern Adriatic are similar to that of a bora [*Zecchetto and Cappa*, 2001; *Dorman et al.*, 2006], which suggests that bora-like wind events had a large influence on the variability of the WAC transport during this time period. This would be consistent with previous findings [*Pullen et al.*, 2003; *Book et al.*, 2005, 2007c; *Ursella et al.*, 2006].

5.6. Model Errors Relative to Observed Currents

[51] Table 3 lists errors for the model currents with respect to the ADCP currents at the moorings at 20-m depth for the period November 2005 through August 2006. The mean and root-mean-square (RMS) errors and the correlation are computed for both the principal and minor variance axis currents. These axes were taken as the mean of the principal and minor variance axes computed for the model and the ADCP currents.

[52] The largest mean current errors at 20 m are at GS3 and GS11 as noted previously, 5.2 and −6.9 cm/s, respectively. At GS11, the model mean current is very small and the model mean current field suggests a shadow zone on the lee current side of Vis Island (Figure 9), whereas the observed mean current at GS11 is fairly large (Figure 5). The RMS error for the principal axis current at the different moorings ranges from 9 to 14 cm/s (which is much larger than the ADCP measurement error, see section 4).

[53] The correlation between the model and ADCP currents is highest near the Italian coast within the WAC along the principal variance axis, which corresponds to the alongshore flow (Figure 5). This is probably due to the constraining effect of the coastline and the dependence of surges in the WAC on the winds as discussed in the previous section.

[54] The correlation of the principal axis current decreases between GS3 and GS7 as the distance from the Italian coast increases. The correlation of the principal axis current increases slightly at GS10 and GS11, perhaps because of the constraining effect of Vis Island, which lies

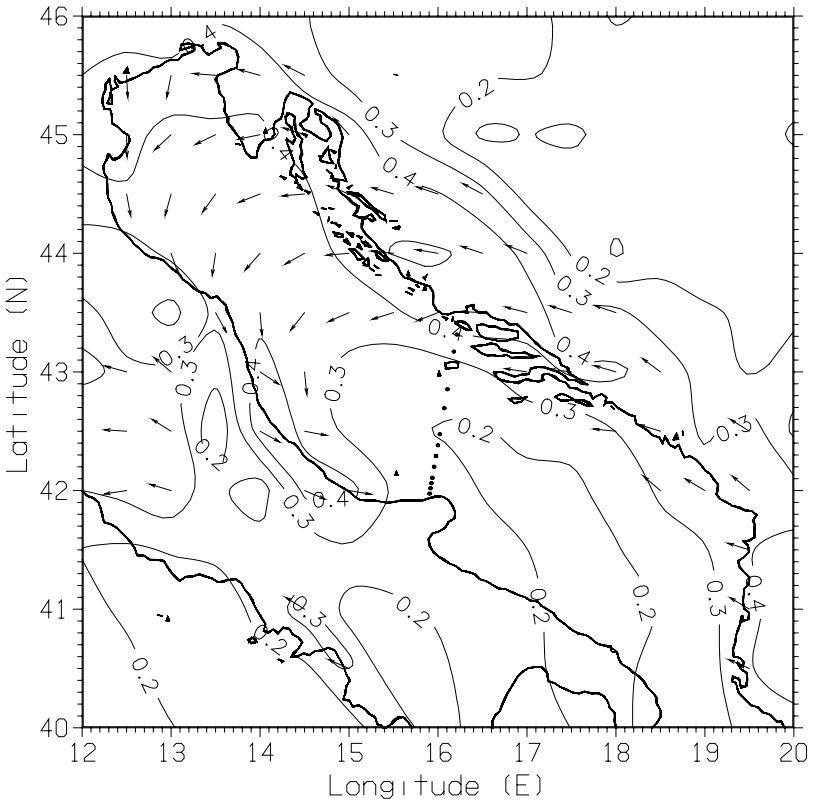

Figure 19. Maximum correlation between ALADIN wind stress forcing and the model transport in the WAC near Gargano Peninsula. Arrows show wind direction associated with the maximum correlation. Black dots indicate mooring locations.

between these two moorings. The low correlation of the current in the interior and along the minor variance axis at all the moorings suggests that particular current instability features, which tend to be small in size because of the small (about 5 km) internal radius of deformation in the Adriatic [*Paschini et al.*, 1993], are not accurately predicted.

5.7. Correlation of ALADIN Winds With Currents at Moorings

[55] Table 5 shows the maximum CC between the ALADIN wind stress and the model and ADCP currents for both the principal and minor variance axes at the GS moorings at 20-m depth. This was computed using a procedure similar to that used to calculate the CC between the ALADIN wind stress and the WAC transport described in section 5.5. The wind stress and current time series were low-pass filtered with a 24-h Butterworth filter, and the CCs listed in Table 5 are the maximum of the values computed for each mooring over all the wind stresses (0.5° bins), wind directions (5° bins), and temporal lags between 0 and 48 h (3-h bins).

[56] For a single CC between filtered time series of these lengths (300 days), correlation values of 0.11 or higher are significant at the 95% confidence level. However, taking the maximum CC over a large number of calculations increases the chance that a nonsignificant CC will exceed 0.11 for one of these and give a false illusion of significant correlation in Table 5. This issue was tested by performing the CC calculations with the current time series reversed in time, which consistently produced maximum CC values of about 0.2. This suggests that maximum CC values near 0.2 in Table 5 should be taken to indicate that there is not much correlation.

[57] Both the model and ADCP currents show roughly similar CC values. The largest correlations ($\geq$0.40) are for the principal variance axes of the currents at GS1–4 near the Italian coast (except for the ADCP principal axis correlation at GS11, which is 0.41). At the interior moorings (GS5–10), the CC values are lower ($\leq$0.32 for the model and $\leq$0.25 for the ADCPs). These results are generally consistent with the correlations between the model and ADCP currents in Table 3; that is, the correlations between the model and ADCP currents are generally higher where

Table 5. Maximum Cross Correlation of ALADIN Wind Stress and Model and ADCP Currents for Both the Principal and Minor Variance Axes at Mooring Locations at 20-m Depth

	Principal Axis		Minor Axis	
Mooring	Model	ADCP	Model	ADCP
GS1	0.74	0.67	0.32	0.29
GS2	0.61	0.44	0.23	0.32
GS3	0.61	0.52	0.13	0.15
GS4	0.41	0.40	0.21	0.14
GS5	0.23	0.19	0.19	0.25
GS6	0.29	0.16	0.21	0.21
GS7	0.25	0.21	0.26	0.29
GS8	0.32	0.22	0.13	0.19
GS9	0.28	0.23	0.23	0.20
GS10	0.29	0.22	0.24	0.20
GS11	0.28	0.41	0.29	0.23
GS12	0.37	0.34	0.13	0.22

the correlations between the winds and the model and ADCP currents are higher.

[58] For the moorings with the larger CC values, the maximum CC within the 0.5° wind stress bins shows a definite spatial structure, with the largest CC values occurring along the Italian coast northwest of Gargano for GS1–3, in the northern Adriatic for GS4, and along the Croatian coast for GS12, which is what might be expected. For the interior moorings, the spatial variation of the maximum CC values is generally uniformly low and does not indicate a specific region of wind influence.

6. Summary

[59] Numerical simulations of the Adriatic Sea were conducted with NCOM during the DART Experiments between October 2005 and September 2006. NCOM was run on a high-resolution, 1-km grid. Model forcing included tides, surface fluxes from the ALADIN atmospheric model, relaxation to a daily satellite SST analysis, extensive river and runoff discharges, and open boundary conditions south of Otranto specified from a global model.

[60] Currents predicted by NCOM were compared with currents from 12 ADCP moorings located along a line between the Gargano Peninsula, Italy and Split, Croatia. Comparison of the model and ADCP tidal currents showed good agreement. Tidal currents at the moorings were generally small and contributed less than 10% to the total variance of the ADCP currents at 10-m depth and less than 20% near the bottom.

[61] Further comparisons were conducted using detided currents. Correlations between the model and ADCP detided currents were highest in the WAC, which flows southeastward along the Italian coast, where the path of the current is somewhat constrained by the coastline. The lowest correlations were at the interior moorings, likely because of instability processes. Consistent with this, correlations between the ALADIN wind stress and the model and ADCP 20-m currents at the mooring locations were highest near the Italian coast and lowest at the interior moorings.

[62] Comparison of current variance also showed best agreement near the Italian and Croatian coasts. In the interior, the model and ADCP mean current variance compared fairly well for November–January, but for February–August the model mean variance decreased significantly relative to the ADCPs and the discrepancy increased with depth. Spectral analyses indicate most of the difference in variance to be at periods greater than 2 days, which suggests that the mesoscale variability predicted by the model in the interior of the Adriatic for February–August is too weak. Some model experiments were conducted to try to find the cause of the discrepancy, but these experiments produced similar results and the cause of the low predicted variance was not determined.

[63] The transport of the WAC was computed from the model and ADCP currents. The mean transport for November 2005 through August 2006 was 0.321 Sv for the model (using just the model currents at the mooring locations) and 0.304 Sv for the ADCP currents. The temporal correlation of these transports is 0.79 for the low-pass (72-h) filtered time series and 0.73 for the unfiltered time series. Correlation of the WAC transport with the ALADIN wind stress over this time period found the highest correlations (>0.4) along the Croatian coast north of Split, along the Italian coast north of Gargano Peninsula, and in the northern Adriatic.

[64] **Acknowledgments.** Thanks to the captains, crews, and scientists of the R/V *G. Dallaporta*, R/V *Alliance*, and R/V *Universitatis* for the successful deployments and recoveries of all the moorings. The success of the mooring effort was in large part due to the dedicated efforts of Mark Hulbert, Andrew Quaid, and Wesley Goode of the NRL technical team. We thank Elio Pachini of CNR-ISMAR-Ancona and Giuseppe Siena of CoNISMa for their respective help during the first deployment and final recovery cruises. Also, thanks to Elio Pachini, Mira Morović, Mirko Orlić, Gordana Beg Paklar, Aniello Russo, and Sandro Carniel for their help with cruise logistics and planning. Michel Rixen of the NATO Undersea Research Centre (NURC) led and organized the larger international DART collaborative project and contributed in many ways to this work. The NRL DART project greatly benefited from being part of a NURC/NRL Joint Research Project and from the larger collaborative effort. Thanks to the reviewers for their useful suggestions. This work was supported by the Office of Naval Research as part of the "Dynamics of the Adriatic in Real-Time" and "Global Remote Littoral Forcing via Deep Water Pathways" research programs (Program Elements 0602435N and 0601153N, respectively). This is NRL contribution NRL/JA/7320–08-8149.

References

Artegiani, A., D. Bregant, E. Paschini, N. Pinardi, F. Raicich, and A. Russo (1997a), The Adriatic Sea general circulation. Part I: Air-sea interaction and water mass structure, *J. Phys. Oceanogr.*, *27*, 1492–1514.

Artegiani, A., D. Bregant, E. Paschini, N. Pinardi, F. Raicich, and A. Russo (1997b), The Adriatic Sea general circulation. Part II: Baroclinic circulation structure, *J. Phys. Oceanogr.*, *27*, 1515–1532.

Barron, C. N., A. B. Kara, H. E. Hurlburt, C. Rowley, and L. F. Smedstad (2004), Sea surface height predictions from the global Navy Coastal Ocean Model (NCOM) during 1998–2001, *J. Atmos. Oceanic Technol.*, *21*(12), 1876–1894.

Barron, C. N., A. B. Kara, P. J. Martin, R. C. Rhodes, and L. F. Smedstad (2006), Formulation, implementation and examination of vertical coordinate choices in the global Navy Coastal Ocean Model (NCOM), *Ocean Modell.*, *11*, 347–375, doi:10.1016/j.ocemod.2005.01.004.

Blumberg, A. F., and G. L. Mellor (1987), A description of a three-dimensional coastal ocean circulation model, in *Three-Dimensional Coastal Ocean Models*, *Coastal and Estuarine Sci.*, vol. 4, edited by N. Heaps, pp. 1–16, AGU, Washington, D. C.

Book, J. W., H. T. Perkins, L. Cavaleri, J. D. Doyle, and J. D. Pullen (2005), ADCP observations of the western Adriatic slope current during winter of 2001, *Prog. Oceanogr.*, *66*, 270–286, doi:10.1029/2003JC001780.

Book, J., M. Rixen, A. Carta, M. Hulbert, A. Quaid, E. Coelho, V. Grandi, and L. Gualdesi (2007a), Shallow water environmental profiler in trawl-resistant real-time configuration (SEPTR) used for frontal dynamics research, *Rapp. Comm. Int. Mer Mediter.*, *38*, 130.

Book, J. W., H. Perkins, R. P. Signell, and M. Wimbush (2007b), The Adriatic Circulation Experiment winter 2002/2003 mooring data report: A case study in ADCP data processing, *NRL Memo. Rep. NRL/MR/7330–07-8999*, U.S. Nav. Res. Lab., Stennis Space Cent., Miss.

Book, J. W., R. P. Signell, and H. Perkins (2007c), Measurements of storm and nonstorm circulation in the northern Adriatic: October 2002 through April 2003, *J. Geophys. Res.*, *112*, C11S92, doi:10.1029/2006JC003556.

Book, J. W., P. J. Martin, I. Janekovic, M. Kuzmic, and M. Wimbush (2009), Vertical structure of bottom Ekman tidal flow: Observatios, theory, and modeling from northern Adriatic, *J. Geophys. Res.*, doi:10.1029/2008JC004736, in press.

Burrage, D. M., J. W. Book, and P. J. Martin (2009), Eddies and filaments of the Western Adriatic Current: Analysis and prediction, *J. Mar. Syst.*, in press.

Carniel, S., M. Sclavo, L. Kantha, and H. Prandke (2008), Double-diffusive layers in the Adriatic Sea, *Geophys. Res. Lett.*, *35*, L02605, doi:10.1029/2007GL032389.

Chavanne, C., I. Janekovic, P. Flament, P.-M. Poulain, M. Kuzmic, and K.-W. Gurgel (2007), Tidal currents in the northwestern Adriatic: High-frequency radio observations and numerical model predictions, *J. Geophys. Res.*, *112*, C03S21, doi:10.1029/2006JC003523.

Courtier, P., and J.-F. Geleyn (1988), A global numerical weather prediction model with variable resolution: Application to the shallow-water equations, *Q. J. R. Meteorol. Soc.*, *114*, 1321–1346.

Cushman-Roisin, B., M. Gacic, P. Poulain, and A. Artegiani (Eds.) (2001), *Physical Oceanography of the Adriatic Sea: Past, Present, and Future*, 304 pp., Kluwer Acad., Dordrecht, Netherlands.

Cushman-Roisin, B., K. A. Korotenko, C. E. Galos, and D. E. Dietrich (2007), Simulation and characterization of the Adriatic Sea mesoscale variability, *J. Geophys. Res.*, *112*, C03S14, doi:10.1029/2006JC003515.

Dorman, C. E., et al. (2006), February 2003 marine atmospheric conditions and the bora over the northern Adriatic, *J. Geophys. Res.*, *111*, C03S03, doi:10.1029/2005JC003134 [printed *112*(C3), 2007].

Dykes, J. D., D. W. Wang, and J. W. Book (2009), An evaluation of a high-resolution operational wave forecasting system in the Adriatic Sea, *J. Mar. Syst.*, in press.

Egbert, G. D., and S. Y. Erofeeva (2003), Efficient inverse modeling of barotropic ocean tides, *J. Atmos. Oceanic Technol.*, *19*, 183–204.

Flather, R. A., and R. Proctor (1983), Prediction of North Sea storm surges using numerical models: Recent developments in the U.K., in *North Sea Dynamics*, edited by J. Sundermann and W. Lenz, pp. 299–317, Springer, New York.

Haza, A. C., et al. (2007), Model-based directed drifter launches in the Adriatic Sea: Results from the DART Experiment, *Geophys. Res. Lett.*, *34*, L10605, doi:10.1029/2007GL029634.

Hendershott, M. C., and P. Rizzoli (1976), The winter circulation in the Adriatic Sea, *Deep Sea Res., Part I*, *23*, 353–370.

Holland, W. R., J. C. Chow, and F. O. Bryan (1998), Application of a third-order upwind scheme in the NCAR Ocean Model, *J. Clim.*, *11*, 1487–1493.

Ivatek-Sahdan, S., and M. Tudor (2004), Use of high-resolution dynamical adaptation in operational suite and research impact studies, *Meteorol. Z.*, *13*, 1–10.

Kondo, J. (1975), Air-sea bulk transfer coefficients in diabatic conditions, *Boundary Layer Meteorol.*, *9*, 91–112.

Korotenko, K. A. (2007), Modeling the mesoscale variability in the Adriatic Sea, *Oceanology*, *47*, 313–324.

Kuzmic, M., I. Janekovic, J. W. Book, P. J. Martin, and J. D. Doyle (2006), Modeling the northern Adriatic double-gyre response to intense bora wind: A revisit, *J. Geophys. Res.*, *111*, C03S13, doi:10.1029/2005JC003377 [printed *112*(C3), 2007].

Lee, C. M., et al. (2005), Northern Adriatic response to a wintertime bora wind event, *Eos Trans. AGU*, *86*, 157.

Martin, P. J. (2000), A Description of the Navy Coastal Ocean Model Version 1.0, *NRL Rep. NRL/FR/7322–00-9962*, 42 pp., Nav. Res. Lab., Stennis Space Cent., Miss.

Martin, P. J., J. W. Book, and J. D. Doyle (2006), Simulation of the northern Adriatic circulation during winter 2003, *J. Geophys. Res.*, *111*, C03S12, doi:10.1029/2006JC003511.

Mellor, G. L. (1991), An equation of state for numerical models of oceans and estuaries, *J. Atmos. Oceanic Technol.*, *8*, 609–611.

Mellor, G. L., and T. Yamada (1974), A hierarchy of turbulence closure models for planetary boundary layers, *J. Atmos. Sci.*, *31*, 1791–1806.

Morey, S. L., P. J. Martin, J. J. O'Brien, A. A. Wallcraft, and J. Zavala-Hidalgo (2003), Export pathways for river discharged fresh water in the northern Gulf of Mexico, *J. Geophys. Res.*, *108*(C10), 3303, doi:10.1029/2002JC001674.

Orlanski, I. (1976), A simple boundary condition for unbounded hyperbolic flows, *J. Comput. Phys.*, *21*, 251–269.

Orlic, M., M. Gacic, and P. E. La Violette (1992), The currents and circulation of the Adriatic Sea, *Oceanol. Acta*, *15*, 109–124.

Orlic, M., M. Kuzmic, and Z. Pasaric (1994), Response of the Adriatic Sea to bora and sirocco forcing, *Cont. Shelf Res.*, *14*, 91–116.

Paschini, E., A. Artegiani, and N. Pinardi (1993), The mesoscale eddy field of the middle Adriatic Sea during fall 1988, *Deep Sea Res., Part I*, *40*, 1365–1377.

Perkins, H., F. de Strobel, and L. Gualdesi (2000), The Barny sentinel trawl-resistant ADCP bottom mount: Design, testing, and application, *IEEE J. Oceanic Eng.*, *25*, 430–436.

Peters, H., C. M. Lee, M. Orlic, and C. E. Dorman (2007), Turbulence in the wintertime northern Adriatic Sea under strong atmospheric forcing, *J. Geophys. Res.*, *112*, C03S09, doi:10.1029/2006JC003634.

Poulain, P. (2001), Adriatic Sea surface circulation as derived from drifter data between 1990 and 1999, *J. Mar. Syst.*, *29*, 3–32.

Pullen, J., J. D. Doyle, R. Hodur, A. Ogston, J. W. Book, H. Perkins, and R. Signell (2003), Coupled ocean-atmosphere nested modeling of the Adriatic Sea during winter and spring 2001, *J. Geophys. Res.*, *108*(C10), 3320, doi:10.1029/2003JC001780.

Querin, S., A. Crise, D. Deponte, and C. Solidoro (2006), Numerical study of role of wind forcing and freshwater buoyancy input on the circulation in a shallow embayment (Gulf of Trieste, Northern Adriatic Sea), *J. Geophys. Res.*, *111*, C03S16, doi:10.1029/2006JC003611.

Raicich, R. (1994), Note on the flow rates of the Adriatic rivers, *Tech. Rep. RF 02/94*, 8 pp., Cons. Naz. delle Ric. Inst. Sper. Talassografico, Trieste, Italy.

Rixen, M., J. Book, P. Martin, N. Pinardi, P. Oddo, J. Chiggiato, and N. Russo (2007), Multi-model super-ensemble ocean prediction: An operational example using a Kalman filter in the Adriatic Sea, *Rapp. Comm. Int. Mer Medit.*, *38*, 188.

Ursella, L., P. Poulain, and R. P. Signell (2006), Surface drifter derived circulation in the northern and middle Adriatic Sea: Response to wind regime and season, *J. Geophys. Res.*, *111*, C03S04, doi:10.1029/2005JC003177.

Zecchetto, S., and C. Cappa (2001), The spatial structure of the Mediterranean Sea winds revealed by ERS-1 scatterometer, *Int. J. Remote Sens.*, *22*, 45–70.

J. W. Book and D. M. Burrage, Ocean Sciences Branch, Oceanography Division, Naval Research Laboratory, Stennis Space Center, MS 39529, USA. (book@nrlssc.navy.mil; derek.burrage@nrlssc.navy.mil)

P. J. Martin and C. W. Rowley, Ocean Dynamics and Prediction Branch, Oceanography Division, Naval Research Laboratory, Stennis Space Center, MS 39529, USA. (paul.martin@nrlssc.navy.mil; clark.rowley@nrlssc.navy.mil)

M. Tudor, Croatian Meteorological and Hydrological Service, Gric 3, HR-10000 Zagreb, Croatia. (tudor@cirus.dhz.hr)